Possible Link of a Structurally Driven Spin Flip Transition and the Insulator-Metal Transition in the Perovskite $La_{1-x}Ba_xCoO_3$

Peng Tong,[1] Juan Yu,[1] Qingzhen Huang,[2] Kazuyoshi Yamada,[3] and Despina Louca[1,*]

[1]*University of Virginia, Department of Physics, Charlottesville, Virginia 22904, USA*

[2]*NIST Center for Neutron Research, Gaithersburg, Maryland 20899, USA*

[3]*WPI Advanced Institute for Materials Research, Tohoku University, Katahira 2-1-1, Aoba, Sendai 980-8577, Japan*

(Received 24 March 2010; revised manuscript received 24 January 2011; published 15 April 2011)

The nature of the magnetic ground state near the insulator-metal transition (IMT) in $La_{1-x}Ba_xCoO_3$ was investigated via neutron scattering. Below the critical concentration, $x_c \sim 0.22$, a commensurate antiferromagnetic (AFM) phase appears initially. Upon approaching x_c, the AFM component weakens and a ferromagnetic (FM) ordered phase sets in while in the rhombohedral lattice. At x_c, a spin flip to a new FM structure occurs at the same time as the crystal symmetry transforms to orthorhombic (*Pnma*). The *Pnma* phase may be the driving force for the IMT.

DOI: 10.1103/PhysRevLett.106.156407 PACS numbers: 71.30.+h, 61.05.fg, 71.70.−d

Exotic magnetic states are ubiquitous in transition metal oxides giving rise to very complex phase diagrams with novel properties. Emerging from the subtle interplay between the electronic and lattice degrees of freedom, their presence has been linked to phenomena such as magnetoelectronic phase separation [1], multiferroicity [2], and geometrical frustration [3]. In the Mott insulating antiferromagnets (AFM) of La_2NiO_4 and La_2CoO_4, for instance, charge doping quickly suppresses the commensurate magnetism, giving way to incommensurate as well as charge ordered states [4,5]. Although their ground states remain insulating, their structures are isomorphic to the La_2CuO_4 doped superconductor and have been instrumental towards understanding the relation between the localization mechanism leading to stripes and superconductivity. In another Mott system, the perovskite cobaltite $LaCoO_3$ where a nonmagnetic insulating ground state is present instead, the consequences from adding holes in the system lead to significantly more complex states. Prior to the crossover from a localized to an itinerant electron behavior [6–10], commonly observed in this class of materials that includes the manganites, competing AFM and ferromagnetic (FM) interactions [11,12] prevail. The origin and organization of these states and the role they play regarding the insulator-metal transition (IMT) is not well understood at present and is the focus of this work. Our results elucidate the significance of magnetoelastic coupling in these cobalt oxides.

The parent compound, the rhombohedral ($R\bar{3}c$) $LaCoO_3$, has an internal spin degree of freedom arising from the nearly degenerate spin states of the Co^{3+} ion that become active due to the comparable Hund's rule exchange and crystal field energies. In the ground state, Co^{3+} is in the low spin (LS) electronic configuration, $t_{2g}^6 e_g^0$ [13]. As the temperature rises, an electronic excitation occurs from the LS state to a higher spin state that fosters the development of dynamic FM and AFM correlations as observed by neutron scattering [14]. Coupled with these interactions are single ion transitions with a characteristic energy of 0.6 meV [14,15]. Upon doping with a divalent ion such as Sr^{2+} or Ba^{2+}, an unusual magnetic state evolves prior to the IMT. In $La_{1-x}Sr_xCoO_3$, the percolation of FM isotropic droplets transforms the system into a long-range metallic ferromagnet (FMM), mediated by double exchange (DE) interactions at a Sr concentration of ~0.18 [9]. Competing, weak incommensurate magnetic correlations found in the insulating state concomitantly with the FM short-range correlations, vanish in the FMM phase [11]. On the other hand, in $La_{1-x}Ba_xCoO_3$, a similar incommensurate state is found which becomes commensurate and long range as the FM short-range correlations become long range, shown in earlier elastic neutron scattering results on single crystals [12]. The magnetic symmetries have not yet been determined, however, and little is known regarding their development beyond IMT [16]. This may be especially important in the Ba system where the itinerant state is decoupled from the FM transition, as will be discussed below.

From neutron powder diffraction measurements in the range of $17\% \leq x \leq 27\%$ that encompass the vicinity of IMT ($x_c \sim 0.22$), we find that coexistence of the two magnetic orders originates in the rhombohedral phase. Initially ($x \sim 0.17$), a commensurate AFM long-range order sets in. A slight increase in x results in the appearance of a FM ordered phase that quickly becomes dominant, while the AFM component weakens and eventually disappears. At x_c and in the complete absence of an AFM signal, a new FM structure develops. Coupled with the appearance of the new magnetic order is a crystal structure transition, from the rhombohedral to an orthorhombic lattice with *Pnma* symmetry. The structurally driven spin flip creates metallic FM droplets and the percolation of these droplets drives the system to become metallic. This, in turn, suggests that the FM domains in the rhombohedral phase are in fact insulating. This is fundamentally distinct

from other magnetoresistive perovskites where only one FM transition is observed prior to the IMT. The cobaltite system is unique as it presents an uncommon mechanism for the IMT in which the actual transition occurs in a two-step process.

The samples were prepared by standard solid state reaction as reported in Ref. [17] and characterized by bulk susceptibility and transport measurements. The neutron powder diffraction data were collected using the BT-1 high resolution powder diffractometer at the NIST Center for Neutron Research. Data for all compositions except $x = 0.18$ were collected using a wavelength of 1.5401 Å from a Cu (311) monochromator while for $x = 0.18$, a wavelength of 2.0784 Å from a Ge (311) monochromator was used.

Figure 1(a) is a plot of intensity as a function of the momentum transfer Q at low temperatures for five of the compositions studied. A list of the atomic and magnetic parameters obtained from the data refinement is given in Table I. In $x = 0.17$, new diffraction peaks are observed that cannot be indexed by the $R\bar{3}c$ nuclear symmetry, their indices labeled in the figure. They are magnetic in origin and can be described by a magnetic propagation vector of $k_1 = (0, -0.5, 0.5)$ [18,19]. This propagation vector corresponds to an AFM spin order. Based on the nuclear symmetry and the observed magnetic propagation vector, it is possible to determine the Co ions spin orientation. There are two Co sites in the $R\bar{3}c$ symmetry, one at (0, 0, 0) that we designate as Co1 and another at (0, 0, 0.5) as Co2. We find that there are two possible spin orientations that could yield the observed magnetic diffraction pattern. In one orientation, the moment basis vectors (m_x, m_y, m_z) along the principle axis of the nuclear cell are (0,1,0) for Co1 and (−1, −1, 0) for Co2. In the second orientation, they are (0, 1, 0) for Co1 and (1, 1, 0) for Co2. Both choices can separately reproduce the AFM diffraction pattern well for $x = 0.17$. Thus the moments are in the $(001)_R$ plane. Other orientations were additionally tested but provided worst fits to the data. Note that from the powder diffraction measurement, it is not possible to distinguish the moment orientation within the ab plane of the $R\bar{3}c$ unit cell. Both orientations described here represent a noncollinear AFM configuration. The case of the second orientation is shown in Fig. 2(a). The AFM unit cell is reproduced by expanding the nuclear unit cell by $2 \times b$ and $2 \times c$.

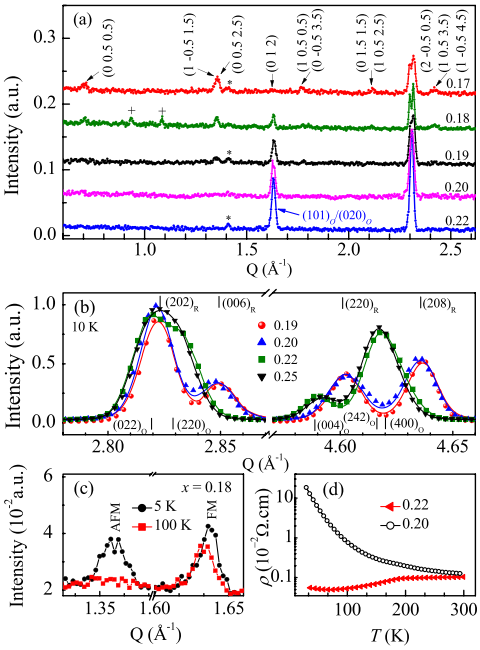

FIG. 1 (color online). (a) The diffraction intensity shown for $x = 0.17 - 0.22$ is normalized to the highest nuclear Bragg peak, $(202)_R$ in $R\bar{3}c$ and $(022)_O$ in $Pnma$. Because of a weak nuclear structure factor, there is little contribution to the peaks at $(012)_R$ in $R\bar{3}c$ and $(101)_O/(020)_O$ in $Pnma$. The intensity of this peak increases with increasing x due to FM correlations. The $\lambda/3(+)$ or $\lambda/2(*)$ contaminations from the BT1 monochromators are marked. (b) A comparison at higher Q values shows the transition from $R\bar{3}c$ ($x \leq 0.20$) to $Pnma$ ($x_c = 0.22$). (c) The temperature dependences of the strongest AFM ($Q \sim 1.36$ Å^{-1}) and FM diffraction ($Q \sim 1.64$ Å^{-1}) peaks for $x = 0.18$. (d) The resistivity for $x = 0.20$ and 0.22 at zero magnetic field.

Indicated in Fig. 1(a) is the Q position of the nuclear $(012)_R$ peak at $Q \sim 1.63$ Å^{-1} that is at the background level in $x = 0.17$ due to its weak nuclear structure factor. But in $x = 0.18$ and $x = 0.19$, the intensity under this Q value is enhanced with the appearance of a FM component with a $k_2 = 0$ wave vector (see Table I). This indicates that the two magnetic components coexist below $x = 0.2$. With increasing x, the intensity under the AFM peaks decreases, and the AFM phase volume fraction is reduced while the FM intensity becomes dominant. We previously showed using single crystals that the FM intensity is isotropic due to the presence of FM droplets [11].

The presence of two magnetic orders in such a narrow region of the phase diagram is perplexing. Based on the nuclear structure refinement at these values of x, no

TABLE I. The refinement results of the nuclear and magnetic structures of $La_{1-x}Ba_xCoO_3$. For $x = 0.17 - 0.20$, the symmetry is $R\bar{3}c$ with lattice constants $a = 5.4593(2)$ Å and $c = 13.2062(1)$ Å in $x = 0.17$, $a = 5.4587(4)$ Å and $c = 13.2186(2)$ Å in $x = 0.18$, and $a = 5.4620(3)$ Å and $c = 13.2295(1)$ Å in $x = 0.20$. In $x = 0.22$, the symmetry is $Pnma$ with lattice constants $a = 5.4309$ Å, $b = 7.6835$ Å, and $c = 5.4765$ Å. The Co-O-Co angle (β), the moment per Co site (μ), and the phase fraction (f) in % in the FM and AFM structures are listed.

x	0.17	0.18	0.20	0.22
β^o	167.13(3)	167.66(8)	167.98(1)	165.89(7) 170.49(4)
f_{AFM}/f_{FM}	100/0	48/52	0/100	0/100
$\mu(\mu B)$	1.20(2)	1.33(1)	1.51(3)	1.65(7)

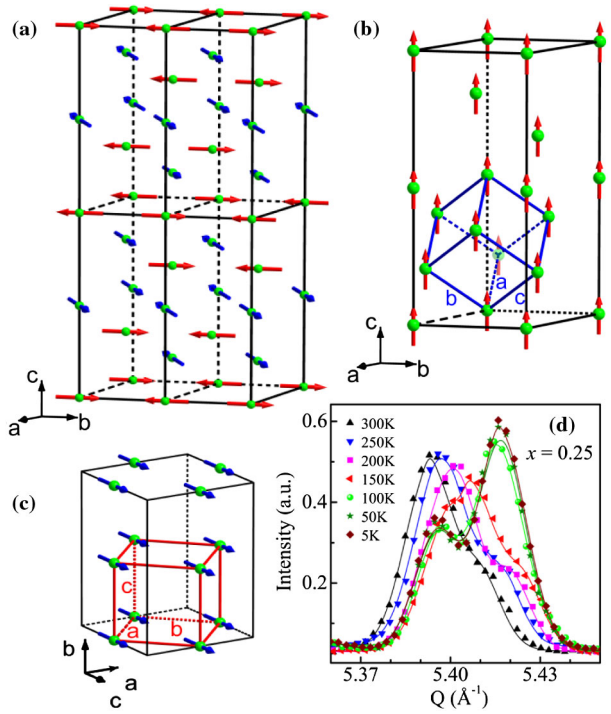

FIG. 2 (color online). (a) The AFM cell in the $R\bar{3}c$ phase. (b) The FM cell in the $R\bar{3}c$ phase. (c) The new FM cell in the *Pnma* phase. (d) The temperature dependence of the diffraction pattern at $x = 0.25$.

evidence is found that can support the presence of two nuclear symmetries that could give rise to two different magnetic states. Figure 1(b) is a plot of the 10 K data for $x = 0.19$ compared to a crystal model with the $R\bar{3}c$ symmetry (solid line). The two magnetic orders either originate from the same magnetic domain or from two different domains [20–22]. It is possible to combine two phases if they originate from the same magnetic domain, and form a double-wave vector magnetic structure. However, if the two phases are independent because they originate from different magnetic domains, forming a single wave vector structure for each domain is more appropriate. The latter was chosen because as seen in Fig. 1(c) for $x = 0.18$, the two phases have different order parameters. The strongest AFM intensity at $Q \sim 1.36$ Å^{-1} shown in this figure almost vanishes by 100 K, while the FM peak at $Q \sim 1.63$ Å^{-1} still persists at this temperature [12]. Note that the nuclear contribution at this position is extremely small and barely visible in the powder data. On cooling, the FM order appears first, followed by the AFM order almost 40° lower. Although the ratio between the AFM to FM intensity changes significantly from $x = 0.18$ to 0.19, their propagation vectors do not change with x. From these observations we deduce that the FM and AFM magnetic orders are weakly coupled, namely, they propagate in different domains [23–25]. To obtain their volume phase fractions as a function of composition, we assumed that the Co magnetic moments in both magnetic phases have the same magnitude, and the sum of their volume fractions was constrained so that it equals that of the nuclear phase fraction [21,22]. The results are listed in Table I.

The magnetic structure of $x = 0.18$ is composed of the AFM model of $x = 0.17$ shown in Fig. 2(a) and the FM model with the $k_2 = 0$ propagation vector shown in Fig. 2(b). In the latter, there are three possible Co spin orientations allowed by symmetry. Of these, only the case where the components of Co1 and Co2 basis vectors are along (0, 0, 1) can reproduce the observed k_2 diffraction pattern. In this configuration, the moments for both Co1 and Co2 point along $(001)_R$ axis as shown in Fig. 2(b). Shown within this cell is the pseudocubic cell with the spins pointing along $(111)_C$ for reference. The refined phase fractions of the AFM and FM phases are 48% and 52%, respectively. If compared to $x = 0.17$ where no FM ordering was observed, a 1% increase in hole concentration led to two comparable magnetic phases. By increasing the concentration further to $x = 0.19$, the AFM fraction is reduced to 17% while the FM fraction increases to 83%. Although by $x = 0.20$, only a FM phase is present, where the FM domains grow in size and the FM coupling strengthens, the system is still insulating as seen from the transport data of Fig. 1(d).

By $x_c = 0.22$, a new FM order sets in due to a spin flip. At this concentration, an IMT is observed as shown in Fig. 1(d). Although the peak intensity at $Q \sim 1.63$ Å^{-1} is enhanced even further [Fig. 1(a)], it corresponds to a new FM phase that appears with a new propagation vector we label $k_3 = 0$. Simultaneously, a crystal structure transition occurs where the nuclear phase changes to the *Pnma* symmetry [26]. Shown in Fig. 2(d) is the temperature dependence of the diffractogram for $x = 0.25$ as it changes with cooling from the rhombohedral to the orthorhombic phase. The solid lines are model fits. A two-phase refinement of the diffraction data between 200–100 K indicates that the volume fraction ratio of $Pnma/R\bar{3}c$ continuously changes. Below 100 K, only the *Pnma* is present. The gradual transition from $R\bar{3}c$ to *Pnma* may couple to the broad IMT transition. This phase persists up to $x \sim 0.27$, above which the $R\bar{3}c$ reappears. In the *Pnma* symmetry, there are four equivalent Co ions with the following basis vectors: Co1: (0, 0, 2); Co2: (0, 0, 2); Co3: (0, 0, 2); Co4: (0, 0, 2), where the moments on all Co ions point along the $(001)_O$ direction as shown in Fig. 2(c). In the pseudocubic cell, the spins point along $(110)_C$, the face diagonal. Thus the spin flips from the $(111)_C$ to the $(110)_C$ direction at the IMT.

The phase diagram in Fig. 3 consists of three distinct regions: the $R\bar{3}c$ insulating (RI) phase below $x = 0.22$, the *Pnma* metallic phase (OM) in the region between $x = 0.22 \sim 0.27$, and the $R\bar{3}c$ metallic (RM) phase at higher x. The RI region is dominated by competing magnetic phases. With increasing x, both types of correlations become long-range ordered. The AFM correlations arise

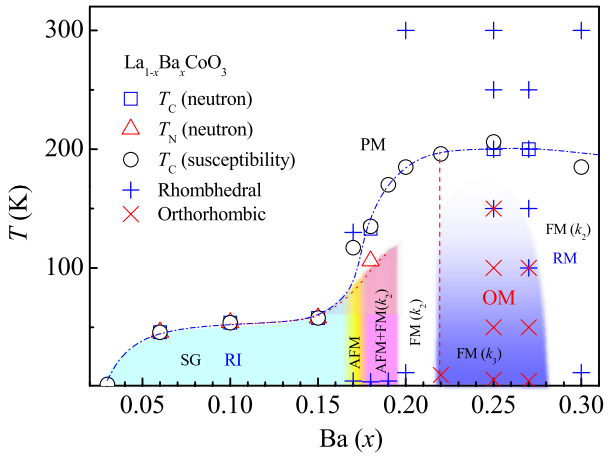

FIG. 3 (color online). The phase diagram of $La_{1-x}Ba_xCoO_3$ ($0.03 \leq x \leq 0.30$) was constructed from neutron and bulk susceptibility measurements. The spin-glass (SG) region consists of short-range correlations. When $x = 0.17$–0.20, AFM and FM phases are established. For $x = 0.2$–0.22, the FM phase is insulating. The structural transition from $R\bar{3}c$ to $Pnma$ at $x = 0.22$ brings about the metallic state.

from superexchange interactions between Co^{3+} ions in the IS state while the FM correlations arise from the DE interactions between Co^{3+} and Co^{4+} ions, the latter introduced with hole doping. Although the AFM order appears first, it is quickly suppressed, for reasons that are not clearly understood at present. To explain this behavior we focus on the nature of the magnetoelastic coupling: in the AFM structure, the antiparallel arrangement of spins lies in the $(111)_C$ [or $(001)_R$] planes. With Ba doping, the distance between the planes increases, weakening the AFM coupling between them. This allows for the AFM spin direction to continuously change from the $(111)_C$ plane to the $(111)_C$ axis. This is supported by the continuous decrease of the volume fraction of the AFM component, leading to the disappearance of the AFM phase by $x = 0.20$ [16]. Upon establishing the FM (k_2) phase, the system does not become metallic as this k_2 structure is decoupled from the IMT. Metallicity appears only after the FM (k_3) state sets in with the structural transition which offers direct evidence for a spin-lattice coupling in cobaltites. From the orbital point of view, in the RI phase ($x = 0.2$), the Co-O-Co bonds are buckled with an angle of 167.98° that reduces orbital overlap. In the OM phase ($x = 0.22$), 2/3 of the bond angles increase to 170.5° in the ab plane while 1/3 reduce to 165.89° along the c axis. This maximizes the Co $3d$ orbital overlap in the ab plane that not only allows for the spins to couple ferromagnetically but also allows for the hopping of charges. In the RM phase above 30%, the bond angle increases to almost 172° which may promote FM DE interactions and the reason for its reappearance.

To summarize, we have shown that the lattice is instrumental to the IMT via the percolation of magnetic droplets that become conductive after a structural transformation that brings on a spin flip to a new magnetic order. The coexistence of the AFM and FM orders as well as the $R\bar{3}c - Pnma$ transition add new insights into the IMT mechanism in $La_{1-x}Ba_xCoO_3$.

This work is supported by the U.S. Department of Energy under Contract No. DE-FG02-01ER45927 and the U.S. DOC through NIST-70NANBH1152.

*To whom correspondence should be addressed.

[1] E. Dagotto, Science **309**, 257 (2005).
[2] M. Mostovoy, Nature Mater. **9**, 188 (2010).
[3] S.-H. Lee *et al.*, J. Phys. Soc. Jpn. **79**, 011004 (2010).
[4] J. M. Tranquada *et al.*, Phys. Rev. Lett. **73**, 1003 (1994).
[5] K. Horigane *et al.*, J. Phys. Soc. Jpn. **76**, 114715 (2007).
[6] C. Zener, Phys. Rev. **82**, 403 (1951).
[7] M. Itoh *et al.*, J. Phys. Soc. Jpn. **63**, 1486 (1994).
[8] M. A. Señaris-Rodríguez and J. B. Goodenough, J. Solid State Chem. **116**, 224 (1995); **118**, 323 (1995).
[9] M. Kriener *et al.*, Phys. Rev. B **69**, 094417 (2004).
[10] P. Mandal *et al.*, Phys. Rev. B **70**, 104407 (2004).
[11] D. Phelan *et al.*, Phys. Rev. Lett. **97**, 235501 (2006).
[12] J. Yu *et al.*, Phys. Rev. B **80**, 052402 (2009).
[13] P. M. Raccah and J. B. Goodenough, Phys. Rev. **155**, 932 (1967).
[14] D. Phelan *et al.*, Phys. Rev. Lett. **96**, 027201 (2006).
[15] A. Podlesnyak *et al.*, Phys. Rev. Lett. **97**, 247208 (2006).
[16] A. P. Sazonov *et al.*, J. Phys. Condens. Matter **21**, 156004 (2009).
[17] D. Phelan *et al.*, Phys. Rev. B **76**, 104111 (2007).
[18] The magnetic structure was refined using the software FULLPROF, J. Rodriguez-Carvajal, Physica (Amsterdam) **192B**, 55 (1993); the basis vectors were calculated using SARAH (A. S. Wills, Physica (Amsterdam) **276B–278B**, 680 (2000)) following the irreducible representation theory.
[19] J. R. Stewart *et al.*, J. Phys. Condens. Matter **19**, 145291 (2007).
[20] E. O. Wollan and W. C. Koehler, Phys. Rev. **100**, 545 (1955).
[21] K. Prokeš *et al.*, Phys. Rev. B **78**, 014425 (2008).
[22] M. Pissas *et al.*, Phys. Rev. B**55**, 397 (1997).
[23] E. Granado *et al.*, Phys. Rev. B **68**, 134440 (2003).
[24] K. J. Thomas *et al.*, Phys. Rev. B **66**, 054415 (2002).
[25] J. Blasco *et al.*, Phys. Rev. B **66**, 174431 (2002).
[26] The enhancement of the Bragg intensity at $Q \sim 1.63$ Å^{-1} should be attributed to FM magnetic scattering rather than the $R\bar{3}c$-$Pnma$ transition, because the corresponding $Pnma$ nuclear structure factor is very weak at that point.